THE JOURNAL OF PHYSICAL CHEMISTRY C

Article

pubs.acs.org/JPCC

Atomic Layer Deposition of Zn(O,S) Alloys Using Diethylzinc with H_2O and H_2S: Effect of Exchange Reactions

Published as part of The Journal of Physical Chemistry virtual special issue "Veronica Vaida Festschrift".

Diane K. Lancaster,[†] Huaxing Sun,[†] and Steven M. George*[,†,‡]

[†]Department of Chemistry and Biochemistry, University of Colorado, Boulder, Colorado 80309, United States

[‡]Department of Mechanical Engineering, University of Colorado, Boulder, Colorado 80309, United States

ABSTRACT: Zn(O,S) thin films have a tunable band gap and are useful as conduction and valence band buffers in various types of solar cells. Previous growth of Zn(O,S) thin films by atomic layer deposition (ALD) has utilized alternating cycles of ZnO ALD and ZnS ALD. Controlling the composition of the Zn(O,S) alloys using alternating cycles is complicated because of an efficient exchange reaction between ZnO and gaseous H_2S given by ZnOH* + H_2S → ZnSH* + H_2O. This facile exchange reaction leads to a higher than expected sulfur content in the Zn(O,S) films. In this study, the effect of this exchange reaction on the composition of Zn(O,S) films was examined by varying the reaction conditions. For growth using alternating cycles, the Zn(O,S) film composition was strongly affected by the temperature and the size of the H_2S exposure. An alternative method that avoids alternating cycles of ZnO ALD and ZnS ALD was also employed to grow Zn(O,S) thin films. This alternative method uses codosing of H_2O and H_2S at 100 °C. Codosing allows the composition of the Zn(O,S) film to be controlled by the mole fraction of the dosing mixture. The relative magnitudes of the exchange reaction rate (k_1) for ZnOH* + H_2S → ZnSH* + H_2O and the competing exchange reaction rate (k_2) for ZnSH* + H_2O → ZnOH* + H_2S could be estimated using this method. Through the study of the composition of the Zn(O,S) films for different H_2O and H_2S partial pressures during codosing, the ratio of the exchange reaction rates, k_1/k_2, was determined to be 71−231. Band gaps were measured for the Zn(O,S) thin films grown using the alternating cycle method and the codosing method. The band gaps could be produced with the most control by varying the mole fraction of H_2S in the H_2S/H_2O codosing mixture.

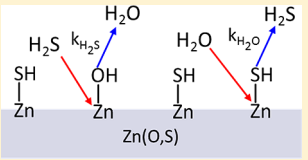

I. INTRODUCTION

Zn(O,S) alloys have received considerable interest because they have tunable band gaps and are useful as conduction and valence band buffers in solar cells.[1] The band gap of Zn(O,S) is tunable from 2.6 to 3.6 eV.[2−10] For Cu(In, Ga)Se_2 solar cells, Zn(O,S) alloys are a potential replacement for the toxic CdS buffer layer.[11,12] For dye-sensitized solar cells, Zn(O,S) alloys could serve as a conduction band buffer between the excited dye molecule and the TiO_2 electron transport layer. The utility of Zn(O,S) alloys depends on the ability to control their composition to tune their band gap and band positions.[13,14]

There are a number of advantages to growing Zn(O,S) alloys using atomic layer deposition (ALD) techniques.[15−17] Ternary alloys can be grown using ALD by alternating the ALD cycles used to grow the pure compounds. The composition of the alloy is controlled by varying the ratio of the ALD cycles used to grow the pure compounds. This alternating cycle method of controlling the composition of ternary alloys is normally very effective. However, there is vast disagreement among the many groups that have studied the relationship between the alloy composition and the ratio of the ZnO/ZnS ALD cycles.[14,16−21] The results for the %ZnS in the Zn(O,S) films versus the fraction of ZnS ALD cycles are shown in Figure 1a. Although there is disagreement between the various results, the ALD growth of Zn(O,S) alloys typically produces films containing far more sulfur than would be predicted by the fraction of ZnS cycles. This higher sulfur content is believed to result from the exchange reaction between H_2S and ZnO.[16]

H_2S can react with the ZnO surface according to

$$\mathrm{ZnOH^* + H_2S \rightarrow ZnSH^* + H_2O} \quad (1)$$

The asterisks indicate the species on the surface. This reaction is similar to the bulk reaction between ZnO and H_2S given by

$$\mathrm{ZnO + H_2S \rightarrow ZnS + H_2O} \quad (2)$$

Thermochemistry predicts that this bulk reaction is exothermic. The standard enthalpy change and standard free energy change are nearly constant at $\Delta H^\circ = -17.5$ kcal and $\Delta G^\circ = -17.5$ kcal, respectively, over a wide temperature range.[22] ΔG predicts a spontaneous reaction until the reaction system reaches an extremely large equilibrium constant of $K = 1.8 \times 10^{10}$ at 100 °C.[22] The reaction of H_2S with ZnO has been well-studied by many previous investigations.[23−27] ZnO is used as an industrial sorbent for hydrogen sulfide. There are many studies on the kinetics and mechanism of this reaction.[23,28−30]

There is also a competing surface reaction where H_2O reacts with ZnSH* according to

$$\mathrm{ZnSH^* + H_2O \rightarrow ZnOH^* + H_2S} \quad (3)$$

Received: June 1, 2017
Revised: July 24, 2017
Published: July 28, 2017

ACS Publications © 2017 American Chemical Society

DOI: 10.1021/acs.jpcc.7b05361
J. Phys. Chem. C 2017, 121, 18643−18652

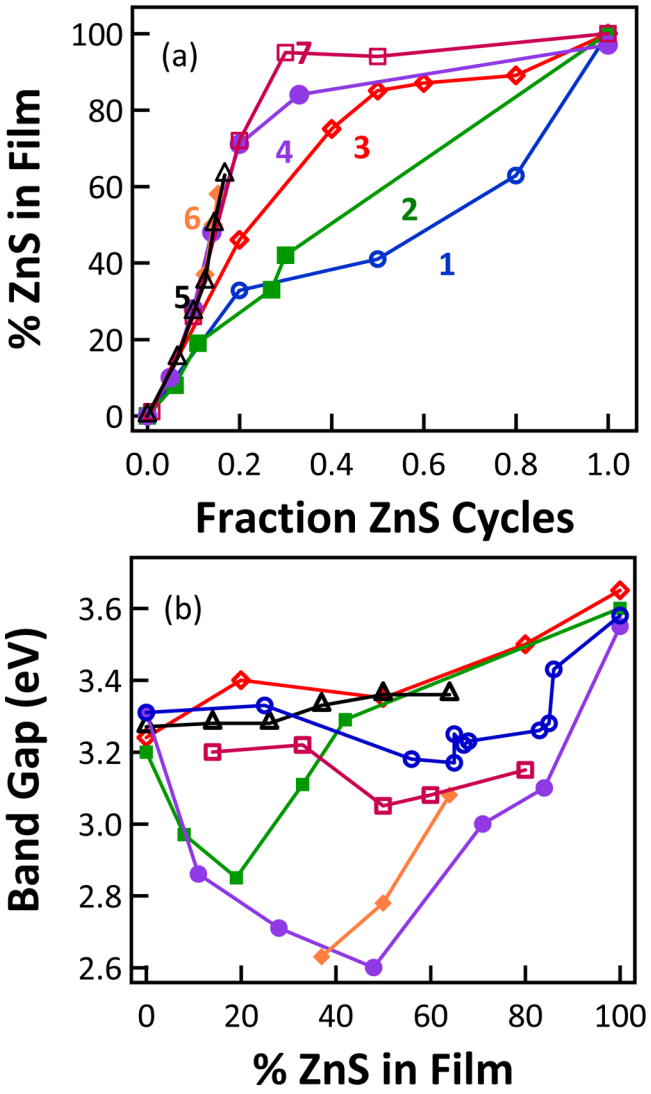

Figure 1. (a) %ZnS in Zn(O,S) film versus fraction of ZnS cycles grown using ALD. (b) Band gaps versus %ZnS in film measured for the same films in panel a. Experimental data from 1 (110 °C),[19] blue circles; 2 (125 °C),[14] green squares; 3 (150 °C),[18] red diamonds (direct transition); 4 (120 °C),[32] purple circles; 5 (120 °C),[20] black triangles; 6 (120 °C),[21] orange diamonds; and 7 (160 °C),[17] maroon squares.

This reaction is similar to the bulk reaction between ZnS and H_2O given by

$$ZnS + H_2O \rightarrow ZnO + H_2S \quad (4)$$

Previous reports have noted the importance of these competing reactions.[16,23,30] The reverse bulk reaction is endothermic with a standard enthalpy change of $\Delta H^\circ = +17.5$ kcal and a standard free energy change of $\Delta G^\circ = +17.5$ kcal.[22] These positive ΔH° and ΔG° values suggest that this reverse reaction is not favorable. However, the H_2O surface reaction during the alternating cycle method is performed with only H_2O in the gas phase. Some H_2O surface reactions will occur to produce a small finite H_2S pressure because ΔG is negative when there is no H_2S partial pressure. The H_2O surface reaction also occurs with ZnSH* surface species and may be very different than the bulk reaction.

There is also a wide variation of band gaps versus the %ZnS in the film reported for Zn(O,S) alloys grown by ALD using the alternating cycle method.[14,16−21] These results are shown in Figure 1b. The reasons for these differences are not clear. Perhaps the various growth strategies produce slightly different film structures. The possible nanolaminate nature of the Zn(O,S) films may be an issue.[31] ZnO, ZnS, and Zn(O,S) alloy films grown by ALD are generally reported to be polycrystalline. The Zn(O,S) films are no longer crystalline when the O/S ratio is ~3/1.[18,32]

In this paper, the growth of Zn(O,S) alloys was examined using in situ quartz crystal microbalance (QCM) to measure the growth rate and ex situ X-ray photoelectron spectroscopy (XPS) and X-ray reflectivity (XRR) techniques to characterize film composition and growth rate. These studies reveal that controlling the composition of Zn(O,S) films using the alternating cycle method is difficult. The temperature, exposure time, and ratio of ZnO/ZnS ALD cycles can strongly affect the composition of the alloy. Zn(O,S) alloys were also grown by codosing the H_2O and H_2S. This alternative growth method is shown to yield more reproducible results for the band gaps than the alternating cycle method. The ratio of the H_2S and H_2O surface exchange reaction rates was also quantified using codosing experiments.

II. EXPERIMENTAL SECTION

Zn(O,S) thin films were grown in a hot-walled viscous flow ALD reactor.[33] The reactor consisted of a stainless steel tube that is 45 cm in length with an inside diameter of 3.5 cm. Two gas lines flowing 75 sccm nitrogen (UHP Airgas) were attached to the front of the reactor. The back of the reactor contained a capacitance manometer pressure gauge and a mechanical pump. Using the nitrogen flow and pumping with the mechanical pump, the pressure in the reactor was ~1 Torr.

Three precursors were used to grow Zn(O,S) thin films: diethyl zinc (DEZ, Sigma-Aldrich), deionized water, and hydrogen sulfide gas (Sigma-Aldrich 99.5% pure). The dose pressure of each precursor, all kept at room temperature, was controlled through a combination of metering valve and two computer-controlled pneumatic valves. Precursors were introduced directly into one of the two nitrogen gas lines and were carried by the N_2 flow into the reactor. During growth using the alternating cycle method, an in situ quartz crystal microbalance was used to monitor the mass of Zn(O,S) thin films.

For ex situ XPS and XRR measurements, thin films were grown on silicon wafers (MEMC, arsenic-doped). For ex situ band gap measurements, Zn(O,S) thin films were deposited on soda-lime glass slide covers (VWR micro cover glass). Prior to deposition, the samples were sonicated in acetone for at least 10 min, rinsed with isopropyl alcohol or methanol, then dried using nitrogen.

Using the alternating cycle method, ZnO, ZnS, and Zn(O,S) thin films were grown using 0.3 s reactant doses followed by 30 s purges. Alloys of ZnO and ZnS were grown by varying the numbers of growth cycles for ZnO ALD using DEZ/H_2O with one cycle for ZnS ALD using DEZ/H_2S. Films grown in this manner were labeled by the ratio of the ZnO:ZnS cycles or by the fraction of ZnS cycles. For example, a 3:1 film was grown using three cycles of ZnO ALD followed by a single cycle of ZnS ALD. A 3:1 film has a ZnS cycle fraction of 0.25.

Most of the Zn(O,S) alloy films were grown at 100 and 150 °C. A few Zn(O,S) alloy films were grown at 225 °C. The precursor exposures were determined from pressure measurements. The peak precursor pressures during the exposures were 60−70 mTorr for H_2O, 30−50 mTorr for H_2S, and 45−55

DOI: 10.1021/acs.jpcc.7b05361
J. Phys. Chem. C 2017, 121, 18643−18652

mTorr for DEZ. The precursor exposures were 0.4−0.5 Torr·s for H_2O, 0.4−0.5 Torr·s for H_2S, and 0.55−0.65 Torr·s for DEZ. All of these exposures are known to grow either ZnO ALD or ZnS ALD at normal growth rates of approximately 2 Å/cycle for ZnO ALD and 1 Å/cycle for ZnS ALD.[34,35] Although DEZ decomposition could be a problem at 225 °C with large DEZ exposures, the decomposition is much slower than the ALD reaction.[36] At the small DEZ exposures used in these experiments, there was no evidence of DEZ decomposition. XPS analysis did not show any carbon or metallic zinc in the Zn(O,S) alloy films grown at 225 °C.

In addition to the alternating growth method, Zn(O,S) films were also grown using the codosing method. The codosing method has also been employed recently to grow Zn(O,S) alloy films using spatial ALD techniques.[37] Codosing replaces the alternating ZnO/ZnS ALD cycles with a single DEZ dose and a combined H_2O/H_2S dose. These films were grown using a quasi-static approach. For these growth experiments, a valve was inserted between the mechanical pump and the reactor that allows for static growth conditions. The reactor was first pumped down to base pressure. The reactor was then isolated from the mechanical pump and exposed to 400−500 mTorr DEZ and held for 5 s. The reactor was then reevacuated to base pressure and purged with 150 sccm N_2 for 35 s.

The substrate was then exposed to the combined H_2O/H_2S dose with the H_2O and H_2S at predetermined pressures. The H_2S mole fraction, X_{H_2S}, was determined from initial partial pressures of H_2O and H_2S by assuming that the gases behave ideally at these low pressures typically less than 1.5 Torr. The H_2O and H_2S pressures were a minimum of 458 mTorr of H_2O and 56 mTorr for H_2S. The precursors were codosed into the reactor and held for 30 s without pumping. To investigate the effect of the initial surface coverage on the final composition and band gap, codosed films were also grown using a slightly different method. A 2 s delay was implemented between the introduction of one of the codosed precursors into the reactor and the second codosed precursor. The delay between the H_2O and H_2S precursors allowed one precursor to react before the other.

Film composition was determined by XPS using a PHI 5600 XPS spectrometer equipped with an Al Kα source. For calibration, four samples were grown using the alternating growth method on glassy carbon substrates. These samples consisted of 1:1, 3:1, 6:1, and 9:1 films. These samples were then analyzed by Rutherford backscattering (RBS) (University of Minnesota Characterization Facility). The RBS calibration determined that the percentage of zinc in the films obtained by the Zn 3s and 3p XPS peak was not reliable. As a result, the % ZnS was determined from XPS analysis using the comparison of the O 1s and S 2s peaks. The film composition determined from the O 1s and S 2s XPS peaks agreed with the RBS analysis for all four films.

X-ray reflectivity was used to determine the thickness of films (Bede D1, Jordan Valley Semiconductors). Band gaps of the films were determined from ultraviolet−visible (UV−vis) transmission measurements using an Ocean Optics ISS-UV/vis. For these measurements, a minimum of 500 cycles yielding film thicknesses of 50−120 nm were grown on soda-lime glass substrates. The band gaps were calculated for direct transitions except for amorphous films where indirect band gaps were determined following standard procedures.[32] Thicker samples were more accurate because there was a persistent optical interference background for thin samples that coincided with the onset of absorption from the band gap.

III. RESULTS AND DISCUSSION

A. Alternating Cycle Method. Figure 2 shows the mass changes monitored by the in situ QCM measurements during the deposition of three Zn(O,S) thin films. These films were grown by alternating cycles with ZnO:ZnS ratios of 9:1, 3:1, and 1:1 at 150 °C. Each of the three alloys has a unique growth pattern. The mass changes reflect the underlying surface reactions occurring during each reactant exposure. In particular, the three alloy films consistently show a larger mass gain for the first H_2S exposure after ZnO ALD cycles than the mass gain for H_2S exposures during steady-state ZnS ALD growth.

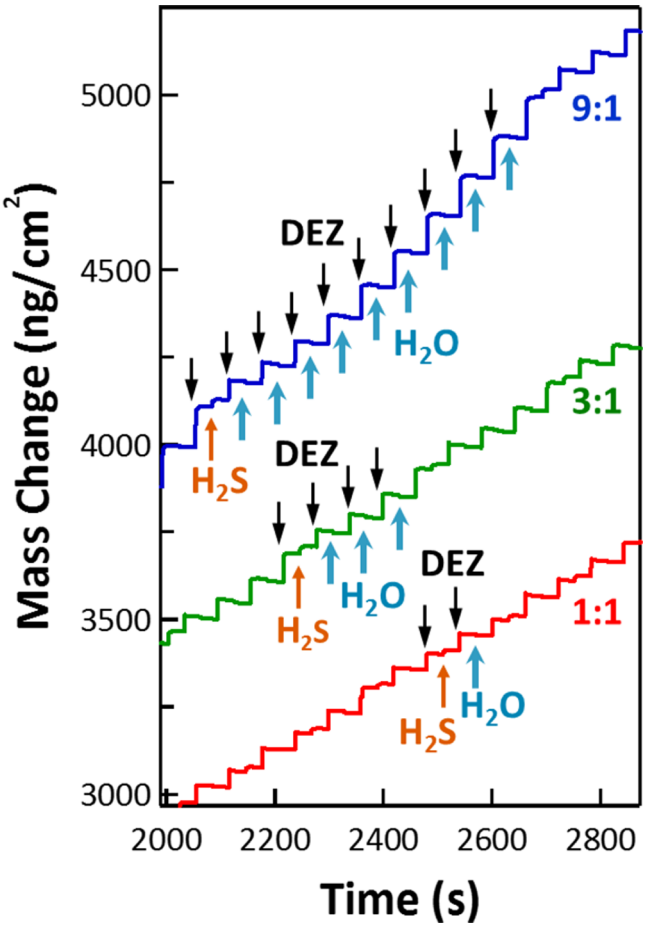

Figure 2. Mass change measured by quartz crystal microbalance during the growth of three Zn(O,S) films: 9:1, 3:1, and 1:1. Orange, blue, and black arrows indicate H_2S, H_2O, and DEZ doses, respectively. Mass changes of the various films have been offset for clarity.

The size of the H_2S mass increase also depends on the number of preceding ZnO cycles. Figure 2 shows that the H_2S mass increases for the first H_2S exposure after the ZnO ALD cycles are 8 ng/cm^2 for the 1:1 film, 27 ng/cm^2 for the 3:1 film, and 30 ng/cm^2 for 9:1 film. In comparison, the mass gains for the DEZ exposures following each H_2S dose are very similar. The DEZ mass increases following the first H_2S exposure after the ZnO ALD cycles are 47, 45, and 48 ng/cm^2 for the 1:1, 3:1, and 9:1 films, respectively.

DOI: 10.1021/acs.jpcc.7b05361
J. Phys. Chem. C 2017, 121, 18643−18652

Experiments can be performed to study the first H_2S exposure after numerous ZnO ALD cycles performed to establish ZnO steady-state growth conditions. The mass change after the first H_2S exposure following ZnO ALD is shown in the upper data set in Figure 3a. The results for ZnS ALD are shown for comparison in the lower data set. An enlargement of the QCM results that highlight the first H_2S exposure following ZnO ALD is shown in Figure 3b. The mass increase for this H_2S exposure is Δm_{H_2S} = 31 ng/cm^2. The mass increase for the subsequent DEZ exposure is Δm_{DEZ} = 49 ng/cm^2. In comparison, the mass increase for the H_2S exposure during ZnS ALD is only Δm_{H_2S} = 2 ng/cm^2. The mass increase for the subsequent DEZ exposure during ZnS ALD is Δm_{DEZ} = 44 ng/cm^2. The total mass change per cycle for ZnS ALD in Figure 3a is Δm = 46 ng/cm^2. This mass change per cycle agrees with previous measurements.[34,35]

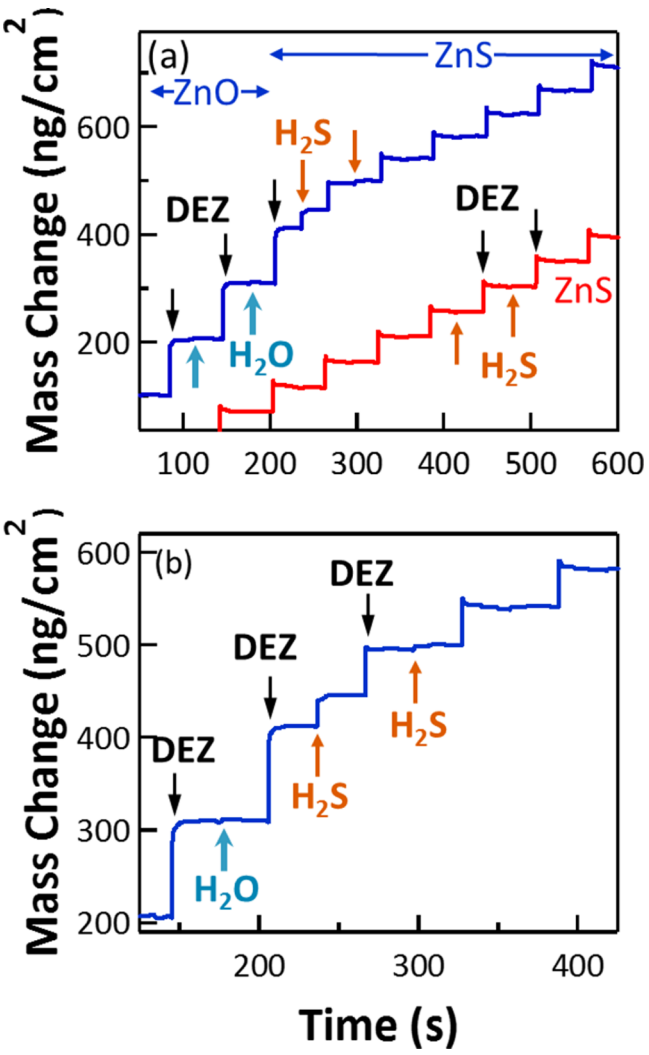

Figure 3. (a) Nucleation of ZnS ALD on ZnO (blue) compared with growth of pure ZnS ALD (red). (b) ZnS ALD nucleation expanded to show initial first two cycles.

The mass increase of Δm_{H_2S} = 31 ng/cm^2 for the first H_2S exposure on the ZnO surface can be used to determine the amount of ZnS produced and the amount of ZnO lost by the H_2S exchange reaction. The mass change for the ZnOH* + H_2S → ZnSH* + H_2O or ZnO + H_2S → ZnS + H_2O exchange reactions is Δm = +16.067 amu = 2.668 × 10^{-23} g. This is the mass change for the conversion of each ZnO to ZnS. The number of ZnO to ZnS conversions can then be calculated by dividing the mass increase of Δm_{H_2S} = 31 ng/cm^2 by the mass change for the conversion of each ZnO to ZnS. The number of ZnO to ZnS conversions is 31 ng/cm^2/2.668 × 10^{-23} g = 1.16 × 10^{15} conversions/cm^2.

The mass per square centimeter of 1.16 × 10^{15} ZnS units per cm^2 is 1.88 × 10^{-7} g/cm^2. This mass per square centimeter divided by the ZnS density of 4.09 g/cm^3 yields a ZnS thickness of 4.6 × 10^{-8} cm or 4.6 Å formed by the exchange reaction. Likewise, the mass per square centimeter of 1.16 × 10^{15} ZnO units per cm^2 is 1.57 × 10^{-7} g/cm^2. This mass per square centimeter divided by the ZnO density of 5.61 g/cm^3 yields a ZnO thickness of 2.8 × 10^{-8} cm or 2.8 Å consumed by the exchange reaction. These calculations indicate that the mass increase of Δm_{H_2S} = 31 ng/cm^2 for the H_2S exposure on the ZnO surface is consistent with losing a ZnO thickness of 2.8 Å and producing a ZnS thickness of 4.6 Å.

The ZnO ALD films are polycrystalline. The ZnO wurtzite structure has lattice constants of a = 3.25 Å and c = 5.2 Å. The loss of 2.8 Å of the ZnO film is slightly less than the loss of one unit cell length. Similarly, the ZnS cubic structure has an edge cell length of 5.41 Å. The production of 4.6 Å of the ZnS film is slightly less than the gain of one unit cell length. The close correspondence of the ZnO thickness loss and ZnS thickness gain and their respective unit cell lengths indicates that the exchange reaction is confined to the top ZnO layer on the ZnO surface.

Similar experiments can also be performed to study the first H_2O exposure after a large number of ZnS ALD cycles performed to establish ZnS steady-state growth conditions. The mass change after the first H_2O exposure following ZnS ALD is shown in the lower data set in Figure 4a. The results for ZnO ALD are shown for comparison in the upper data set. An enlargement of the QCM results that highlight the first H_2O exposures following ZnS ALD is shown in Figure 4b. The mass loss for the first H_2O exposure is Δm_{H_2O} = −6 ng/cm^2. The mass increase for the subsequent DEZ exposure is Δm_{DEZ} = 48 ng/cm^2. In comparison, the mass loss for H_2O exposures during ZnO ALD in the steady-state growth region is Δm_{H_2O} = −2 ng/cm^2. The mass increase for the steady-state DEZ exposure is Δm_{DEZ} = 113 ng/cm^2. The total mass change per cycle for ZnO ALD in Figure 4a is Δm = 111 ng/cm^2. This mass change per cycle agrees with previous measurements.[38,39]

Approximately nine cycles are required for ZnO ALD to reach steady-state growth conditions following ZnS ALD. The Δm_{DEZ} mass gains for the DEZ exposures steadily increase during this nucleation period. The larger Δm_{DEZ} mass gains would be expected to lead to larger Δm_{H_2O} mass losses following H_2O exposures. However, the opposite trend is observed during the nucleation of ZnO ALD on ZnS. This behavior suggests that the larger mass loss of Δm_{H_2O} = −6 ng/cm^2 for the first H_2O exposure after ZnS ALD is associated with the exchange reaction: ZnSH* + H_2O → ZnOH* + H_2S or ZnS + H_2O → ZnO + H_2S.

The exchange reactions affect the composition of the Zn(O,S) alloys grown using alternating ZnO ALD and ZnS ALD cycles. The composition of the Zn(O,S) alloys is much more sulfur-rich than would be predicted from a "rule of mixtures" prediction.[40] This behavior indicates that the H_2S

DOI: 10.1021/acs.jpcc.7b05361
J. Phys. Chem. C 2017, 121, 18643−18652

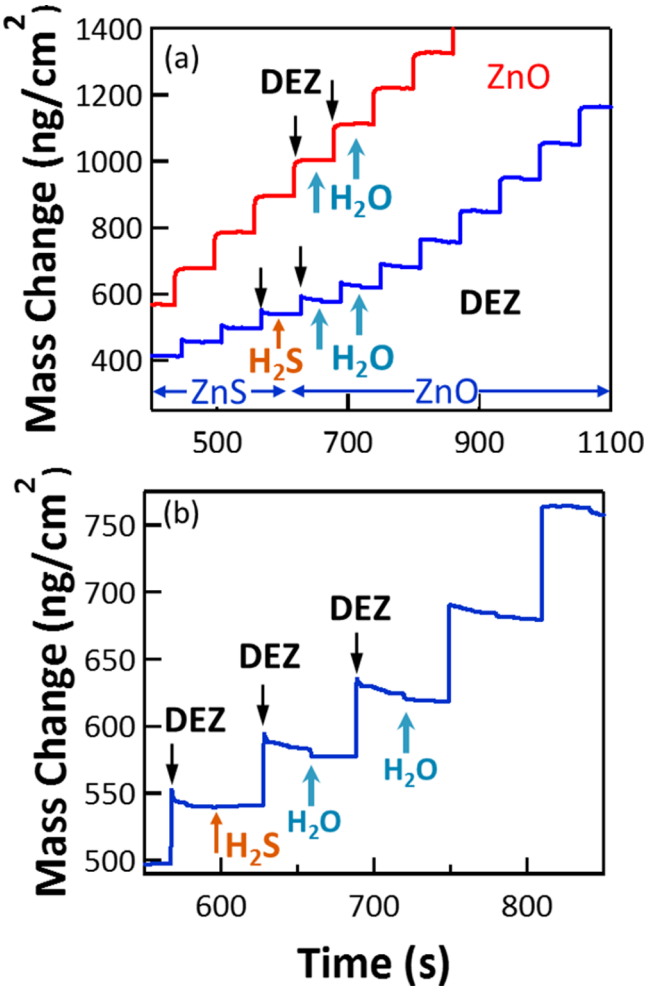

Figure 4. (a) Nucleation of ZnO ALD on ZnS (blue) compared with growth of pure ZnO ALD (red). (b) ZnO ALD nucleation expanded to show initial first two cycles.

exchange reaction has a disproportionate effect on the Zn(O,S) alloy composition. XPS results for the Zn(O,S) film composition are shown in Figure 5. Results are shown for three different growth temperatures: 100 °C, 150 °C, and 225 °C. The %ZnS in the film is determined by the O 1s and S 2p XPS peaks. Figure 5 indicates that there is much more sulfur than expected from the fraction of ZnS ALD cycles. Similar sulfur-rich films were observed in the previous studies displayed in Figure 1a.

Figure 5 also shows that the %ZnS in the films increases rapidly over a narrow range of growth conditions. At 150 °C, the %ZnS varies with fraction of ZnS cycles from 21% ZnS at 8:1 to 73% at 3:1. In addition, Figure 5 indicates that higher growth temperatures increase the measured sulfur content. Zn(O,S) alloys grown at a 3:1 ratio of ZnO to ZnS cycles have %ZnS compositions of 65% at 100 °C, 75% at 150 °C, and 90% at 225 °C. This behavior suggests that there are more efficient H_2S exchange reactions at higher temperatures. At 150 °C, the Zn(O,S) films reach 95% ZnS at a 1:1 ratio of ZnO to ZnS cycles.

The size of the H_2S exposure also affects the %ZnS composition. The %ZnS in Zn(O,S) alloys grown at 150 °C using a 4:1 ratio of ZnO and ZnS ALD cycles versus H_2S exposure is displayed in Figure 6. The H_2S exposures were increased by varying the exposure pressure with the H_2S

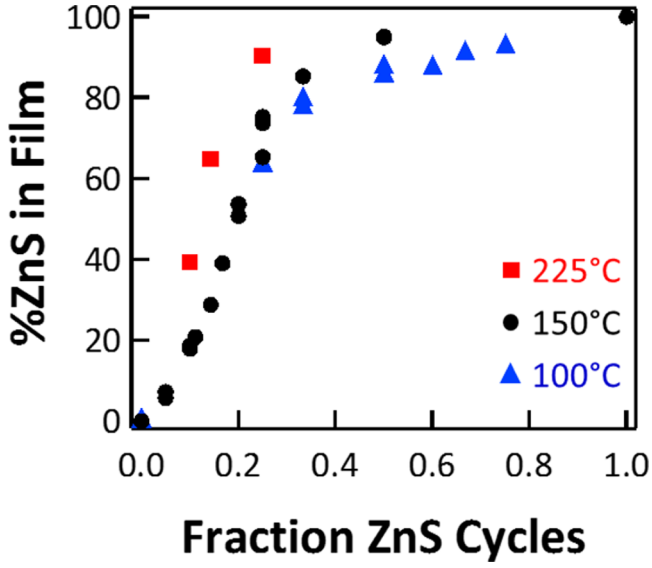

Figure 5. %ZnS in Zn(O,S) films grown using alternating cycles of ZnS ALD and ZnO ALD at 100, 150, and 225 °C.

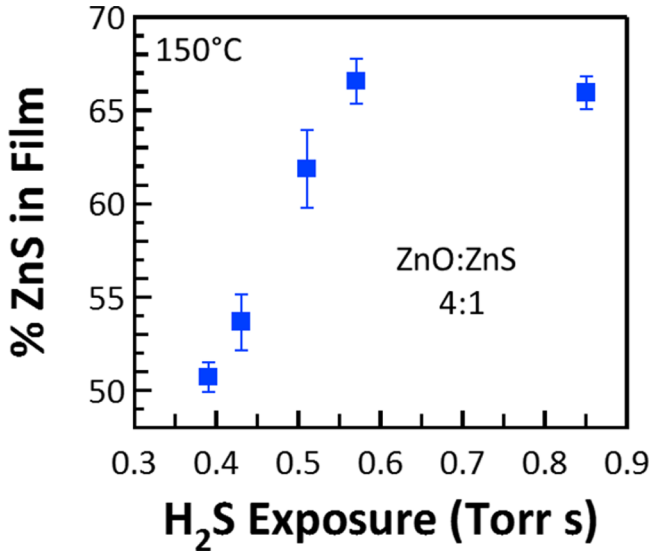

Figure 6. %ZnS in 4:1 Zn(O,S) film versus H_2S exposure at 150 °C.

exposure time at 0.3 s. The %ZnS in the film increases with H_2S exposure until the %ZnS reaches a plateau at larger H_2S exposures. The %ZnS increases from 51% ZnS at 0.39 Torr·s to 66% ZnS at 0.57 Torr·s. A film of pure ZnS would be grown using a 0.3 Torr·s exposure. This trend for %ZnS versus H_2S exposure for the 4:1 films was also observed for the 3:1 and 2:1 Zn(O,S) films. This dependence of the %ZnS composition on the H_2S exposure suggests that the H_2S exposures undergo the exchange reaction with ZnO until most of the oxygen has been exchanged with sulfur on the surface of the Zn(O,S) alloy. At this point, larger H_2S exposures do not lead to higher %ZnS composition.

B. Codosing Method. Zn(O,S) films were also grown by combining the H_2O and H_2S exposures and codosing the two reactants using static exposures. These Zn(O,S) films were grown using DEZ and H_2O/H_2S mixtures at 100 °C. The H_2O/H_2S mixture was allowed to remain in contact with the surface for 30 s. Figure 7 shows that Zn(O,S) film growth is extremely linear using the codosing method for a mole fraction

DOI: 10.1021/acs.jpcc.7b05361
J. Phys. Chem. C 2017, 121, 18643−18652

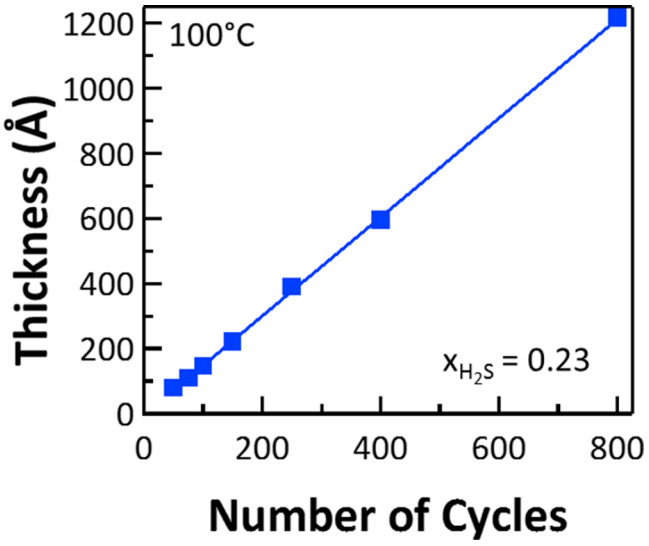

Figure 7. Thickness of Zn(O,S) film versus number of cycles for codosing with a H_2S mole fraction of X_{H_2S} = 0.23 at 100 °C.

of H_2S in the gas mixture of X_{H_2S} = 0.23. The growth rate was 1.5 Å/cycle and the %ZnS composition was 98.5%. This growth rate is significantly higher than the growth rate of 1.0 Å/cycle typical for ZnS ALD.[34]

Figure 8 shows the relationship between the %ZnS in the Zn(O,S) alloy and the mole fraction of H_2S in the gas mixture.

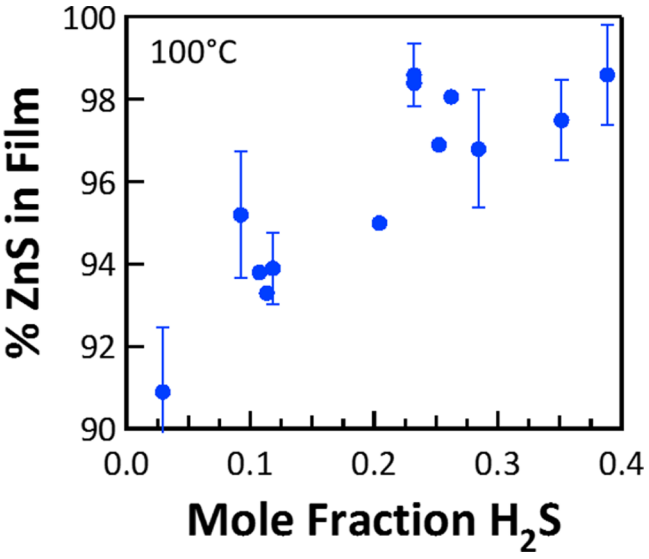

Figure 8. %ZnS in Zn(O,S) films for codosing versus mole fraction of H_2S at 100 °C.

The %ZnS increases with increasing H_2S mole fraction in the combined H_2O/H_2S mixture. Note that the range of %ZnS is quite small and varies from only 91% to 99% in Figure 8. Although there is some scatter in the data, the scatter is only a few percent and probably results from the O 1s and S 2p XPS peak analysis.

The codosing was performed by introducing H_2O and H_2S gases into the reactor at the same time. To explore the effect of reactant timing, a 2 s delay was intentionally added between the introduction of either H_2O or H_2S into the reactor. This delay allowed the initial reaction to take place exclusively with either H_2O or H_2S prior to the introduction of the second precursor. Delaying the input of H_2O by 2 s after the input of H_2S produced Zn(O,S) films with a %ZnS composition that was <1% greater than the %ZnS composition resulting from delaying the H_2S by 2 s after the input of H_2O. The comparable compositions of the two films suggest that they both reach a similar state regardless of their initial state.

Band gaps of Zn(O,S) films calculated from UV−vis transmission spectra are shown in Figure 9. These Zn(O,S)

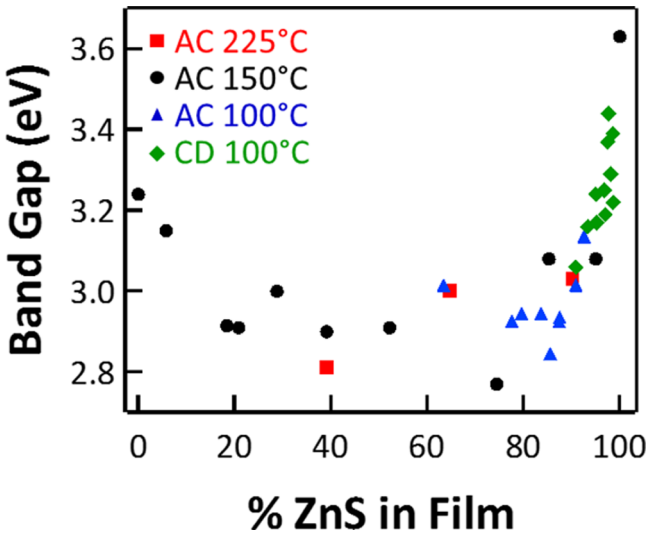

Figure 9. Band gaps for Zn(O,S) films versus %ZnS in film. Films were grown by alternating cycles at 100 °C (blue triangles), 150 °C (black circles), and 225 °C (red squares) and by codosing at 100 °C (green diamonds).

films were grown at 100, 150, and 225 °C using the alternating cycle (AC) method and at 100 °C using the codosing (CD) method. The measured band gaps for ZnO of 3.23 eV and ZnS of 3.63 eV agree with previous measurements for ALD films.[18] These band gaps are close to the bulk crystalline band gaps of ZnO at 3.3 eV and ZnS at 3.54 eV. The growth temperature does not greatly affect the magnitude of the band gap. Although there is some scatter, the band gaps for Zn(O,S) films grown at the different temperatures are in general agreement.

The Zn(O,S) films grown at 150 °C span the widest range of %ZnS composition. The band gaps of these Zn(O,S) films grown at 150 °C follow a roughly parabolic shape. This distinct "bowing" is consistent with the bowing observed for other Zn(O,S) films deposited by other methods[3,41] The minimum band gap occurs at 2.77 eV in the region of 20−80%ZnS where the change in %ZnS does not greatly affect the band gap. This broad band gap minimum is different than most of the previous measurements displayed in Figure 1b for the band gap of Zn(O,S) alloys grown by ALD.[2,32]

Films with band gaps between 3.23 eV (ZnO) and 3.63 eV (ZnS) could not be produced from the alternating cycle method. These large band gaps could be obtained only for films grown using the codosing method. The alternating cycle method does not have the control needed to tune the %ZnS composition over a narrow range of high sulfur composition. Controlling the %ZnS composition between 90 and 99% is extremely difficult because the H_2S exchange reaction increases the %ZnS composition. In addition, films at high %ZnS composition are problematic for the alternating cycle method.

DOI: 10.1021/acs.jpcc.7b05361
J. Phys. Chem. C 2017, 121, 18643−18652

At low ZnO:ZnS ratios of <1:10, the films are more likely to be heterogeneous and should be viewed as nanolaminates instead of homogeneous films.[31]

The band gaps of the Zn(O,S) films as a function of %ZnS grown using the codosing method are shown in Figure 10. The

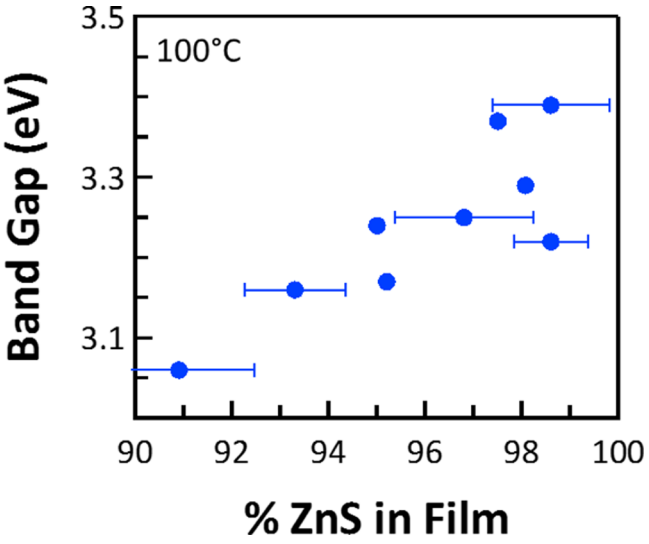

Figure 10. Band gaps for Zn(O,S) films versus %ZnS in film for films grown by codosing at 100 °C.

band gap is moderately linear as a function of %ZnS. There is scattering of the band gap values that may be related to the uncertainty in the %ZnS composition. This uncertainty in the %ZnS composition is attributed to the difficulty obtaining accurate oxygen-to-sulfur ratios from the O 1s and S 2s XPS signals when the O 1s signals are low.

Figure 11 shows the band gaps of the Zn(O,S) films grown using the codosing method as a function of the mole fraction of H_2S in the H_2O/H_2S mixture. In contrast to the scattering in Figure 10 between the band gap and %ZnS values caused by uncertainty in the %ZnS composition, the band gaps in Figure 11 are linear with the mole fraction of H_2S in the dosing

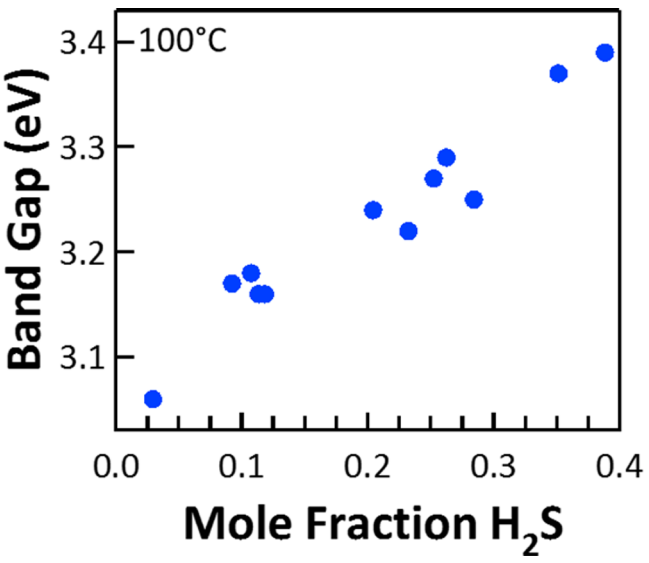

Figure 11. Band gaps for Zn(O,S) films versus mole fraction of H_2S for films grown by codosing at 100 °C.

mixture. The mole fraction of H_2S in the dosing mixture is controlling the %ZnS composition much more accurately than can be determined from the XPS analysis. This control of the % ZnS composition yields excellent control of the band gap.

C. Modeling the Exchange Reactions Yielding Film Composition. The H_2S exchange reaction plays a dominant role in determining the composition of the Zn(O,S) alloys. To obtain more understanding of this H_2S exchange reaction, a model was developed to characterize the H_2S exchange reactions during codosing experiments. The model assumes that the Zn(O,S) film composition reaches a steady-state value when exposed to the H_2S and H_2O gas mixture.

The film composition is assumed to result from kinetic processes that define the rate of change of the Θ_S and Θ_O surface coverages. k_{H_2S} is the rate constant for the exchange of the surface oxygen with sulfur by H_2S (eq 1). k_{H_2O} is the rate constant for the exchange of surface sulfur with oxygen by H_2O (eq 3). Θ_S and Θ_O are the fractional surface coverages of sulfur and oxygen, respectively, where $\Theta_S + \Theta_O = 1$. A schematic illustrating the H_2S and H_2O exchange reactions on a Zn(O,S) film is shown in Figure 12.

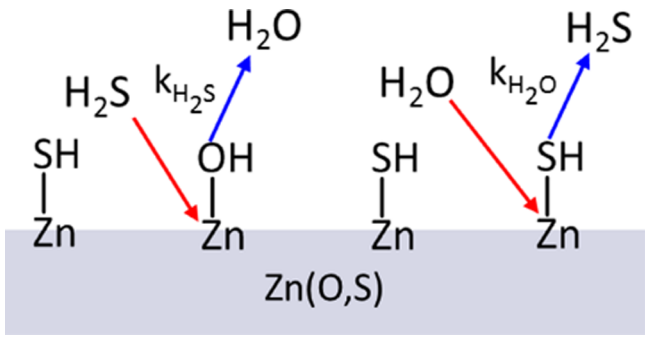

Figure 12. Schematic showing H_2S and H_2O exchange reactions on Zn(O,S) film.

The kinetic processes governing the rates of change of the Θ_S and Θ_O coverages are as follows:

$$\frac{d\theta_S}{dt} = k_{H_2S}P_{H_2S}\theta_O - k_{H_2O}P_{H_2O}\theta_S = -\frac{d\theta_O}{dt} \quad (5)$$

$$\theta_S = \theta_{S,i} + \frac{d\theta_S}{dt} \quad (6)$$

$$\theta_O = 1 - \theta_S \quad (7)$$

P_{H_2S} and P_{H_2O} are the initial pressures of H_2S and H_2O in the reactor at the start of each codose exposure. The initial pressures are assumed to remain constant throughout the reaction.

To calculate a final sulfur coverage, $\Theta_{S,f}$, the initial sulfur coverage is assumed to be $\Theta_{S,i} = 0$. The rate equations are then iterated until there is convergence on a constant Θ_S value. To determine k_{H_2O}, the k_{H_2S} is fixed and the k_{H_2O} value is varied until the $\Theta_{S,f}$ value matches the measured %ZnS value determined by the XPS analysis. A constant, Q, can then be determined by the ratio of k_{H_2S} and k_{H_2O}.

$$Q = \frac{k_{H_2S}}{k_{H_2O}} \quad (8)$$

DOI: 10.1021/acs.jpcc.7b05361
J. Phys. Chem. C 2017, 121, 18643−18652

Experiments and modeling were conducted for H_2S mole fractions in the H_2S and H_2O gas mixture ranging from X_{H_2S} = 0.07 to X_{H_2S} = 0.39. These H_2S mole fractions were obtained using a wide range of partial pressures for H_2S and H_2O. Table 1 also lists the %ZnS composition for the Zn(O,S) films grown

Table 1. X_{H_2S}, P_{H_2S}, P_{H_2O}, %ZnS, and Q Values

X_{H_2S}	P_{H_2S} (Torr)	P_{H_2O} (Torr)	%ZnS	Q
0.07	0.07	0.86	93.8	189
0.09	0.06	0.55	95.2	194
0.11	0.07	0.55	93.3	109
0.112	0.08	0.61	93.9	114
0.20	0.14	0.54	95	74
0.23	0.22	0.74	98.6	231
0.23	0.22	0.74	98.4	200
0.25	0.28	0.83	96.9	93
0.26	0.50	1.40	98.1	143
0.28	0.19	0.48	96.8	75
0.35	0.31	0.58	97.5	71
0.39	0.29	0.46	98.6	111

using these H_2S mole fractions determined by XPS analysis. There is some correlation between the H_2S mole fractions and the %ZnS compositions. In addition, Table 1 reports the values of Q for different Zn(O,S) films grown using the codosing method. The values of Q vary from 71 to 231.

The equilibrium constant corresponding to $\Delta G^\circ = -17.5$ kcal for the bulk reaction $ZnO + H_2S \rightarrow ZnS + H_2O$ given by eq 2 at 100 °C is $K = 1.8 \times 10^{10}$.[22] This equilibrium constant is orders of magnitude larger than Q = 71−231 determined by the kinetic model. This disparity can be attributed to the differences between the surface and bulk reactions. The Q value represents the ratio of rate constants for the surface reactions given by eqs 1 and 3. These surface exchange reactions are primarily between H_2S and hydroxyl groups and H_2O and thiol groups, as shown in Figure 12. These reactions take place in the top layer of the surface. The QCM measurements indicated that the H_2S exchange reaction with the ZnO surface leads to the loss of ZnO from the top 2.8 Å of the initial ZnO film and the production of ZnS in the top 4.6 Å of the final film. The surface reactions result in exchange over distances slightly less than the unit cell lengths for ZnO and ZnS.

The equilibrium constant, K, represents the ratio of the rates of the bulk reactions given by eqs 2 and 4. The equilibrium constant does not account for kinetic barriers that may exist for the surface reactions. The surface exchange reactions may have reaction cross sections that are not correlated with the bulk thermodynamics. The surface reactions are also performed with initial mole fractions of H_2S and H_2O that are far from equilibrium. Because of the limited conversion for the exchange reactions restricted to the top layer of the surface, there may be no possibility to establish equilibrium conditions.

The Q values do not appear to correlate with any of the parameters in Table 1. The range of Q values from 71 to 231 is partially attributed to the uncertainty of the %ZnS composition values from XPS analysis. %ZnS compositions that are higher than the real %ZnS composition would lead to k_{H_2S} and Q values that are higher than the real Q values. %ZnS compositions that are lower than the real %ZnS composition would lead to k_{H_2S} and Q values that are lower than the real Q values.

The Q values indicate that the k_{H_2S} rate constant is 71−231 times higher than the k_{H_2O} rate constant. This larger k_{H_2S} rate constant is expected from the favorable thermochemistry of the H_2S exchange reaction. The codosing experiments provide a means to determine the relative exchange rate constants. These relative rate constants would be difficult to measure by other experimental means. Molecular beam surface scattering experiments could provide an alternative method.

D. Exchange in Other Surface Reactions. The exchange of sulfur and oxygen by the $ZnOH^* + H_2S \rightarrow ZnSH^* + H_2O$ surface reaction is one example of many other surface exchange reactions. These reactions are driven, in part, by the favorable thermochemistry of the exchange process. These exchange reactions can convert the surface layer to a more thermodynamically favorable reaction product. These surface reactions may be prevalent during a wide range of surface reactions.[42]

Surface exchange reactions can also explain observations during Al_2O_3 ALD or HfO_2 ALD on various compound semiconductors surfaces.[43,44] During the exchange reactions, the TMA or hafnium precursors replace the initial surface oxide on the semiconductor surface with Al_2O_3 or HfO_2, respectively. These reactions have been defined as interfacial "self-cleaning" reactions because they remove the initial surface oxide that is detrimental to electrical performance of the dielectric film on the semiconductor substrate.[45] These exchange reactions are proposed during Al_2O_3 ALD on the initial surface oxides of GaAs,[45] InP,[46] and InSb.[47] Similar exchange reactions are believed to occur during HfO_2 ALD on the initial surface oxides of GaAs[45,48] and InGaAs.[49]

Other surface exchange reactions have been reported where the metal in the initial metal oxide is exchanged to produce another metal oxide. One prominent example is the reaction of TMA with ZnO according to $3ZnO + 2Al(CH_3)_3 \rightarrow Al_2O_3 + 3Zn(CH_3)_2$.[38,50] This exchange reaction has been observed during the growth of ZnO/Al_2O_3 nanolaminates.[38,51] Additional surface exchange reactions occur where the metal in an initial metal sulfide is exchanged to produce another metal sulfide. Examples of these exchange reactions include DEZ reacting with In_2S_3 or Cu_2S to produce ZnS.[42,52,53]

Most of the surface exchange reactions have been observed during thin-film growth by ALD. Surface exchange can also occur during surface etching processes. For example, TMA exchange reactions can convert ZnO to Al_2O_3 during thermal ZnO atomic layer etching (ALE).[54] This exchange reaction mechanism is referred to as "conversion-etch".[54] TMA exchange reactions can also convert SiO_2 to Al_2O_3 and aluminosilicates during the thermal SiO_2 ALE reaction mechanism.[55] The conversion of SiO_2 to Al_2O_3 may also occur during Al_2O_3 ALD on SiO_2 surfaces.[56] Atomic layer processing by ALD and ALE is expected to yield many more examples of surface exchange mechanisms.

V. CONCLUSIONS

Zn(O,S) thin films were grown using atomic layer deposition (ALD) techniques to produce tunable band gaps. Alternating cycles of ZnO ALD and ZnS ALD were initially used to deposit the Zn(O,S) films. The composition of the Zn(O,S) alloys deposited using the alternating cycle method was not easy to control. The problem is an efficient surface exchange reaction

DOI: 10.1021/acs.jpcc.7b05361
J. Phys. Chem. C 2017, 121, 18643−18652

between ZnO and gaseous H_2S given by ZnOH* + H_2S → ZnSH* + H_2O. This exchange reaction produces much higher sulfur content in the Zn(O,S) films than expected based on the ratio of ZnO ALD and ZnS ALD cycles. The effect of the exchange reaction on the composition of Zn(O,S) films grown using alternating cycles was examined by varying the reaction conditions. These experiments revealed that the sulfur content was higher in Zn(O,S) films grown at higher temperatures and with longer H_2S exposures.

An alternative method of growing the Zn(O,S) thin films was then explored that uses codosing of H_2O and H_2S at 100 °C. This codosing method produced different compositions of the Zn(O,S) film by varying the mole fraction of the dosing mixture. The codosing method controlled the Zn(O,S) alloy composition much more accurately than the alternating cycle method. The band gaps for Zn(O,S) thin films were measured using the alternating cycle or codosing method. The band gaps could be produced with the most control by the mole fraction of H_2S in the H_2O/H_2S codosing mixture.

The relative magnitudes of the exchange reaction rate (k_1) for ZnOH* + H_2S → ZnSH* + H_2O and the competing exchange reaction rate (k_2) for ZnSH* + H_2O → ZnOH* + H_2S were also determined using the codosing method. A model was used to determine the ratio of the exchange reaction rates, $Q = k_1/k_2$, based on the composition of the Zn(O,S) films grown using the codosing method with different H_2O and H_2S partial pressures. The ratio of the exchange reaction rates was determined to be $Q = 71-231$. This ratio is consistent with a much more efficient exchange reaction for H_2S with ZnOH* than for H_2O with ZnSH*. Surface exchange reactions are possible because of favorable thermochemistry and may be fairly ubiquitous during atomic layer processing.

AUTHOR INFORMATION

ORCID

Steven M. George: 0000-0003-0253-9184

Notes

The authors declare no competing financial interest.

ACKNOWLEDGMENTS

This research was funded by the SunShot Program of the U.S. Department of Energy through a subcontract from Sandia National Laboratories in Livermore, California. The authors acknowledge useful discussions with Dr. Mark Allendorf at Sandia National Laboratories in Livermore, California, and Dr. Erik Spoerke at Sandia National Laboratories in Albuquerque, New Mexico.

REFERENCES

(1) van Delft, J. A.; Garcia-Alonso, D.; Kessels, W. M. M. Atomic Layer Deposition for Photovoltaics: Applications and Prospects for Solar Cell Manufacturing. *Semicond. Sci. Technol.* **2012**, *27*, 074002.

(2) Sanders, B. W.; Kitai, A. Zinc Oxysulfide Thin Films Grown by Atomic Layer Deposition. *Chem. Mater.* **1992**, *4*, 1005−1011.

(3) Polity, A.; Meyer, B. K.; Krämer, T.; Wang, C.; Haboeck, U.; Hoffmann, A. ZnO Based Ternary Transparent Conductors. *Phys. Status Solidi A* **2006**, *203*, 2867−2872.

(4) Jaquez, M.; Yu, K. M.; Ting, M.; Hettick, M.; Sánchez-Royo, J. F.; Wełna, M.; Javey, A.; Dubon, O. D.; Walukiewicz, W. Growth and Characterization of $ZnO_{1-x}S_x$ Highly Mismatched Alloys Over the Entire Composition. *J. Appl. Phys.* **2015**, *118*, 215702.

(5) Khomyak, V.; Shtepliuk, I.; Khranovskyy, V.; Yakimova, R. Band-Gap Engineering of $ZnO_{1-x}S_x$ Films Grown by RF Magnetron Sputtering of ZnS Target. *Vacuum* **2015**, *121*, 120−124.

(6) Meyer, B. K.; Polity, A.; Farangis, B.; He, Y.; Hasselkamp, D.; Krämer, T.; Wang, C.; Haboeck, U.; Hoffmann, A. On the Composition Dependence of $ZnO_{1-x}S_x$. *Phys. Status Solidi C* **2004**, *1*, 694−697.

(7) Pan, H. L.; Yang, T.; Yao, B.; Deng, R.; Sui, R. Y.; Gao, L. L.; Shen, D. Z. Characterization and Properties of $ZnO_{1-x}S_x$ Alloy Films Fabricated by Radio-Frequency Magnetron Sputtering. *Appl. Surf. Sci.* **2010**, *256*, 4621−4625.

(8) Pandey, S. K.; Pandey, S.; Parashar, V.; Yadav, R. S.; Mehrotra, G. K.; Pandey, A. C. Bandgap Engineering of Colloidal Zinc Oxysulfide via Lattice Substitution with Sulfur. *Nanoscale* **2014**, *6*, 1602−6.

(9) Thankalekshmi, R. R.; Rastogi, A. C. Structure and Optical Band Gap of $ZnO_{1-x}S_x$ Thin Films Synthesized by Chemical Spray Pyrolysis for Application in Solar Cells. *J. Appl. Phys.* **2012**, *112*, 063708.

(10) Xu, H.; Zhu, L.; Jiang, J.; Cai, H.; Chen, W.; Hu, L.; Guo, Y.; Ye, Z. Wavelength Tunable Photoluminescence of $ZnO_{1-x}S_x$ Alloy Thin Films Grown by Reactive Sputtering. *J. Appl. Phys.* **2013**, *114*, 083522.

(11) Bakke, J. R.; Pickrahn, K. L.; Brennan, T. P.; Bent, S. F. Nanoengineering and Interfacial Engineering of Photovoltaics by Atomic Layer Deposition. *Nanoscale* **2011**, *3*, 3482−508.

(12) Naghavi, N.; Abou-Ras, D.; Allsop, N.; Barreau, N.; Bücheler, S.; Ennaoui, A.; Fischer, C. H.; Guillen, C.; Hariskos, D.; Herrero, J.; Klenk, R.; Kushiya, K.; Lincot, D.; Menner, R.; Nakada, T.; Platzer-Björkman, C.; Spiering, S.; Tiwari, A. N.; Törndahl, T. Buffer Layers and Transparent Conducting Oxides for Chalcopyrite Cu(In,Ga)-$(S,Se)_2$ Based Thin Film Photovoltaics: Present Status and Current Developments. *Prog. Photovoltaics* **2010**, *18*, 411−433.

(13) Hultqvist, A.; Platzer-Björkman, C.; Coronel, E.; Edoff, M. Experimental Investigation of $Cu(In_{1-x},Ga_x)Se_2/Zn(O_{1-z},S_z)$ Solar Cell Performance. *Sol. Energy Mater. Sol. Cells* **2011**, *95*, 497−503.

(14) Kobayashi, T.; Kumazawa, T.; Jehl Li Kao, Z.; Nakada, T. $Cu(In,Ga)Se_2$ Thin Film Solar Cells with a Combined ALD-Zn(O,S) Buffer and MOCVD-ZnO:B Window Layers. *Sol. Energy Mater. Sol. Cells* **2013**, *119*, 129−133.

(15) Nakashima, K.; Kumazawa, T.; Kobayashi, T.; Mise, T.; Nakada, T. Wide-Gap $Cu(In,Ga)Se_2$ Solar Cells with Zn(O,S) Buffer Layers Prepared by Atomic Layer Deposition. *Jpn. J. Appl. Phys.* **2012**, *51*, 10NC15.

(16) Platzer-Björkman, C.; Törndahl, T.; Abou-Ras, D.; Malmström, J.; Kessler, J.; Stolt, L. Zn(O,S) Buffer Layers by Atomic Layer Deposition in $Cu(In,Ga)Se_2$ Based Thin Film Solar Cells: Band Alignment and Sulfur Gradient. *J. Appl. Phys.* **2006**, *100*, 044506.

(17) Yousfi, E. B.; Asikainen, T.; Pietu, V.; Cowache, P.; Powalla, M.; Lincot, D. Cadmium-Free Buffer Layers Deposited by Atomic Layer Epitaxy for Copper Indium Diselenide Solar Cells. *Thin Solid Films* **2000**, *361-362*, 183−186.

(18) Bakke, J. R.; Tanskanen, J. T.; Hägglund, C.; Pakkanen, T. A.; Bent, S. F. Growth Characteristics, Material Properties, and Optical Properties of Zinc Oxysulfide Films Deposited by Atomic Layer Deposition. *J. Vac. Sci. Technol., A* **2012**, *30*, 01A135.

(19) Jeon, S.; Bang, S.; Lee, S.; Kwon, S.; Jeong, W.; Jeon, H.; Chang, H. J.; Park, H.-H. Characteristics of Zinc-Oxide-Sulfide-Mixed Films Deposited by Using Atomic Layer Deposition. *J. Korean Phys. Soc.* **2008**, *53*, 3287−3295.

(20) Park, H. H.; Jayaraman, A.; Heasley, R.; Yang, C.; Hartle, L.; Mankad, R.; Haight, R.; Mitzi, D. B.; Gunawan, O.; Gordon, R. G. Atomic Layer Deposition of Al-Incorporated Zn(O,S) Thin Films with Tunable Electrical Properties. *Appl. Phys. Lett.* **2014**, *105*, 202101.

(21) Sun, L.; Haight, R.; Sinsermsuksakul, P.; Bok Kim, S.; Park, H. H.; Gordon, R. G. Band Alignment of SnS/Zn(O,S) Heterojunctions in SnS Thin Film Solar Cells. *Appl. Phys. Lett.* **2013**, *103*, 181904.

(22) Kim, Y. Y.; Lim, W. S.; Park, J. B.; Yeom, G. Y. Layer by Layer Etching of the Highly Oriented Pyrolythic Graphite by Using Atomic Layer Etching. *J. Electrochem. Soc.* **2011**, *158*, D710−D714.

(23) Efthimiadis, E. A.; Sotirchos, S. V. Reactivity Evolution During Sulfidation of Porous Zinc Oxide. *Chem. Eng. Sci.* **1993**, *48*, 829−843.

(24) Lew, S.; Sarofim, A. F.; Flytzani-Stephanopoulos, M. Sulfidation of Zinc Titanate and Zinc Oxide Solids. *Ind. Eng. Chem. Res.* **1992**, *31*, 1890−1899.

DOI: 10.1021/acs.jpcc.7b05361
J. Phys. Chem. C 2017, 121, 18643−18652

(25) Novochinskii, I. I.; Song, C.; Ma, X.; Liu, X.; Shore, L.; Lampert, J.; Farrauto, R. J. Low-Temperature H_2S Removal from Steam-Containing Gas Mixtures with ZnO for Fuel Cell Application. 1. ZnO Particles and Extrudates. *Energy Fuels* **2004**, *18*, 576−583.
(26) Rodriguez, J. A.; Chaturvedi, S.; Kuhn, M.; Hrbek, J. Reaction of H_2S and S_2 with Metal/Oxide Surfaces: Band-Gap Size and Chemical Reactivity. *J. Phys. Chem. B* **1998**, *102*, 5511−5519.
(27) Rosso, I.; Galletti, C.; Bizzi, M.; Saracco, G.; Specchia, V. Zinc Oxide Sorbents for the Removal of Hydrogen Sulfide from Syngas. *Ind. Eng. Chem. Res.* **2003**, *42*, 1688−1697.
(28) Davidson, M. J.; Lawrie, C. H.; Sohail, K. Kinetics of Absorption of Hydrogen Sulfide by High Purity and Doped High Surface Area Zinc Oxide. *Ind. Eng. Chem. Res.* **1995**, *34*, 2981−2989.
(29) Neveux, L.; Chiche, D.; Perez-Pellitero, J.; Favergeon, L.; Gay, A. S.; Pijolat, M. New Insight into the ZnO Sulfidation Reaction: Mechanism and Kinetics Modeling of the ZnS Outward Growth. *Phys. Chem. Chem. Phys.* **2013**, *15*, 1532−45.
(30) Samokhvalov, A.; Tatarchuk, B. J. Characterization of Active Sites, Determination of Mechanisms of H_2S, COS and CS_2 Sorption and Regeneration of ZnO Low-Temperature Sorbents: Past, Current and Perspectives. *Phys. Chem. Chem. Phys.* **2011**, *13*, 3197−209.
(31) Lee, D.-J.; Kim, H.-M.; Kwon, J.-Y.; Choi, H.; Kim, S.-H.; Kim, K.-B. Structural and Electrical Properties of Atomic Layer Deposited Al-Doped ZnO Films. *Adv. Funct. Mater.* **2011**, *21*, 448−455.
(32) Persson, C.; Platzer-Bjorkman, C.; Malmstrom, J.; Torndahl, T.; Edoff, M. Strong Valence-Band Offset Bowing of $ZnO_{1-x}S_x$ Enhances p-Type Nitrogen Doping of ZnO-Like Alloys. *Phys. Rev. Lett.* **2006**, *97*, 146403.
(33) Elam, J. W.; Groner, M. D.; George, S. M. Viscous Flow Reactor with Quartz Crystal Microbalance for Thin Film Growth by Atomic Layer Deposition. *Rev. Sci. Instrum.* **2002**, *73*, 2981−2987.
(34) Tanskanen, J. T.; Bakke, J. R.; Pakkanen, T. A.; Bent, S. F. Influence of Organozinc Ligand Design on Growth and Material Properties of ZnS and ZnO Deposited by Atomic Layer Deposition. *J. Vac. Sci. Technol., A* **2011**, *29*, 031507.
(35) Yousfi, E. B.; Fouache, J.; Lincot, D. Study of Atomic Layer Epitaxy of Zinc Oxide by In-Situ Quartz Crystal Microgravimetry. *Appl. Surf. Sci.* **2000**, *153*, 223−234.
(36) Ferguson, J. D.; Weimer, A. W.; George, S. M. Surface Chemistry and Infrared Absorbance Changes During ZnO Atomic Layer Deposition on ZrO_2 and $BaTiO_3$ Particles. *J. Vac. Sci. Technol., A* **2005**, *23*, 118−125.
(37) Frijters, C. H.; Poodt, P.; Illiberi, A. Atmospheric Spatial Atomic Layer Deposition of Zn(O,S) Buffer Layer for Cu(In,Ga)Se_2 Solar Cells. *Sol. Energy Mater. Sol. Cells* **2016**, *155*, 356−361.
(38) Elam, J. W.; George, S. M. Growth of ZnO/Al_2O_3 Alloy Films Using Atomic Layer Deposition Techniques. *Chem. Mater.* **2003**, *15*, 1020−1028.
(39) Riha, S. C.; Libera, J. A.; Elam, J. W.; Martinson, A. B. Design and Implementation of an Integral Wall-Mounted Quartz Crystal Microbalance for Atomic Layer Deposition. *Rev. Sci. Instrum.* **2012**, *83*, 094101.
(40) Callister, W. D.; Rethwisch, D. G. *Materials Science and Engineering: An Introduction*, 9th ed.; John Wiley & Sons, Inc.: Hoboken, NJ, 2014.
(41) Meyer, B. K.; Polity, A.; Farangis, B.; He, Y.; Hasselkamp, D.; Krämer, T.; Wang, C. Structural Properties and Bandgap Bowing of $ZnO_{1-x}S_x$ Thin Films Deposited by Reactive Sputtering. *Appl. Phys. Lett.* **2004**, *85*, 4929−4931.
(42) Genevee, P.; Donsanti, F.; Schneider, N.; Lincot, D. Atomic Layer Deposition of Zinc Indium Sulfide Films: Mechanistic Studies and Evidence of Surface Exchange Reactions and Diffusion Processes. *J. Vac. Sci. Technol., A* **2013**, *31*, 01A131.
(43) Gougousi, T. Atomic Layer Deposition of High-k Dielectrics on III-V Semiconductor Surfaces. *Prog. Cryst. Growth Charact. Mater.* **2016**, *62*, 1−21.
(44) Klejna, S.; Elliott, S. D. First-Principles Modeling of the "Clean-Up" of Native Oxides during Atomic Layer Deposition onto III-V Substrates. *J. Phys. Chem. C* **2012**, *116*, 643−654.
(45) Hinkle, C. L.; Sonnet, A. M.; Vogel, E. M.; McDonnell, S.; Hughes, G. J.; Milojevic, M.; Lee, B.; Aguirre-Tostado, F. S.; Choi, K. J.; Kim, H. C.; Kim, J.; Wallace, R. M. GaAs Interfacial Self-cleaning by Atomic Layer Deposition. *Appl. Phys. Lett.* **2008**, *92*, 071901.
(46) Brennan, B.; Dong, H.; Zhernokletov, D.; Kim, J.; Wallace, R. M. Surface and Interfacial Reaction Study of Half Cycle Atomic Layer Deposited Al_2O_3 on Chemically Treated InP Surfaces. *Appl. Phys. Express* **2011**, *4*, 125701.
(47) Hou, C. H.; Chen, M. C.; Chang, C. H.; Wu, T. B.; Chiang, C. D.; Luo, J. J. Effects of Surface Treatments on Interfacial Self-cleaning in Atomic Layer Deposition of Al_2O_3 on InSb. *J. Electrochem. Soc.* **2008**, *155*, G180−G183.
(48) Suri, R.; Lichtenwalner, D. J.; Misra, V. Interfacial Self Cleaning During Atomic Layer Deposition and Annealing of HfO_2 Films on Native (100)-GaAs Substrates. *Appl. Phys. Lett.* **2010**, *96*, 112905.
(49) Chang, C. H.; Chiou, Y. K.; Chang, Y. C.; Lee, K. Y.; Lin, T. D.; Wu, T. B.; Hong, M.; Kwo, J. Interfacial Self-cleaning in Atomic Layer Deposition of HfO_2 Gate Dielectric on $In_{0.15}Ga_{0.85}As$. *Appl. Phys. Lett.* **2006**, *89*, 242911.
(50) Elam, J. W.; Libera, J. A.; Pellin, M. J.; Stair, P. C. Spatially Controlled Atomic Layer Deposition in Porous Materials. *Appl. Phys. Lett.* **2007**, *91*, 243105.
(51) Na, J. S.; Peng, Q.; Scarel, G.; Parsons, G. N. Role of Gas Doping Sequence in Surface Reactions and Dopant Incorporation during Atomic Layer Deposition of Al-Doped ZnO. *Chem. Mater.* **2009**, *21*, 5585−5593.
(52) Genevee, P.; Donsanti, F.; Renou, G.; Lincot, D. Study of Growth Mechanism and Properties of Zinc Indium Sulfide Thin Films Deposited by Atomic Layer Chemical Vapor Deposition over the Entire Range of Composition. *J. Phys. Chem. C* **2011**, *115*, 17197−17205.
(53) Thimsen, E.; Peng, Q.; Martinson, A. B. F.; Pellin, M. J.; Elam, J. W. Ion Exchange in Ultrathin Films of Cu_2S and ZnS under Atomic Layer Deposition Conditions. *Chem. Mater.* **2011**, *23*, 4411−4413.
(54) Zywotko, D. R.; George, S. M. Thermal Atomic Layer Etching of ZnO by a "Conversion-Etch" Mechanism Using Sequential Exposures of Hydrogen Fluoride and Trimethylaluminum. *Chem. Mater.* **2017**, *29*, 1183−1191.
(55) DuMont, J. W.; Marquardt, A. E.; Cano, A. M.; George, S. M. Thermal Atomic Layer Etching of SiO_2 by a "Conversion-Etch" Mechanism Using Sequential Reactions of Trimethylaluminum and Hydrogen Fluoride. *ACS Appl. Mater. Interfaces* **2017**, *9*, 10296−10307.
(56) Lamagna, L.; Wiemer, C.; Perego, M.; Spiga, S.; Rodriguez, J.; Coll, D. S.; Grillo, M. E.; Klejna, S.; Elliott, S. D. Mechanisms for Substrate-Enhanced Growth during the Early Stages of Atomic Layer Deposition of Alumina onto Silicon Nitride Surfaces. *Chem. Mater.* **2012**, *24*, 1080−1090.

NOTE ADDED AFTER ASAP PUBLICATION

This paper was published on August 17, 2017. Figure 1 has been corrected and the paper was re-posted on August 22, 2017.

DOI: 10.1021/acs.jpcc.7b05361
J. Phys. Chem. C 2017, 121, 18643−18652